WCTE 2016
World Conference on Timber Engineering
August 22-25, 2016 | Vienna, Austria

AN INNOVATIVE HYBRID TIMBER STRUCTURE IN JAPAN: PERFORMANCE OF COLUMN AND BEAMS

Shinichi Shioya[1], Takeshi Koga[2], Yuto Kumon[3], Kazuaki Otsuki [4], Kouhei Uchimura [5]

ABSTRACT: In this paper, bending behaviours in hybrid composite glulam timbers reinforced using deformed steel bars and epoxy resin adhesives (RGTSB) are presented. The technique RGTSB was developed in order to improve flexural stiffness and strength in glulam timbers composed of rapid grown Japanese cedars. A 2:3-scaled column and two half-scaled column-beam assemblies were tested under reversed cyclic loading. Force-displacement curves, hysteresis loops, flexural strain distributions, observations on failure on the tests, are described. Numerical-analysis results are reported to predict force-displacement hysteresis loops until failure of the column and beams using a software for reinforced concrete members and structures.

KEYWORDS: hybrid composite timber, glulam timber, steel bar, column, beam, Japanese cedar, seismic

1 INTRODUCTION

Japanese cedar is one of rapid grown species, which was planted much in Japan, 5-6 decades ago. In Japan, there is, at present, a biggest concern about utilizing the cedars as structural glulam products for timber structure. However, most of the cedars are low-grade on stiffness and strength for structural members, due to the rapid growth.

On the other hand, many designers desire innovative timber members and their structural systems for buildings, with slender members such as reinforced concrete or steel members.

One of reinforcement techniques for Japanese cedar's glulam timbers would be using deformed steel bars (deformed bars) and adhesives, which improve flexural stiffness and strength in timber members [1-2].

Shioya, i.e. one of authors, proposed the structural system and the construction for buildings, with Reinforced Glulam Timber Structure system using Steel Bars (RGTSB, nicknamed "Samurai" in Japan)[3]; developed the structural design methodology; constructed the first prototype building with two-way frame structure, which is one lower story with l8m long-span beams using the RGTSB system in cooperation with Yamasa Mokuzai Corp. at Kagoshima pref. in Japan, on July in 2014, as shown in Figure 1.

The building was designed by Shioya, with a national approval of structural design at Building Centre of Japan; has been used as a stock-yard building for glulam products at Yamasa Mokuzai Corp.

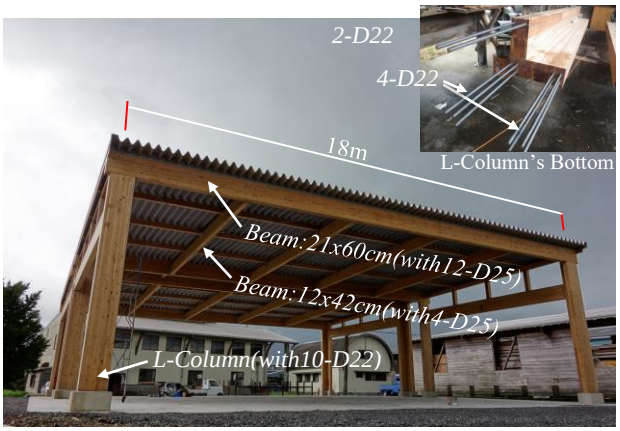

Figure 1: *The first prototype building utilizing RGTSB "Samurai", July 2014*

In order to develop further RGTSB structural system, the following experiments were conducted:

1) beams subjected to monotonic and reversed cyclic bending and shear [3]; 2) column-beam connections with rigidity for portal frame; 3) joint method of deformed bars embedded inside of the glulam timbers with carbon fibre plastic sleeves(CFPSs) and epoxy resin adhesives; 4) long-term loading beams to reveal the effect of deformed bars suppressing flexural creep deflection in the timbers[4]; 5) one column connected to reinforced concrete foundation, subjected to reversed cyclic horizontal load; 6) beam-to-beam connections for longer span beams than 13m, generally a limit in Japan to covey

[1] Shinichi Shioya, Department of Architecture and Architectural Engineering, Kagoshima University, Kagoshima, Japan, shin@aae.kagoshima-u.ac.jp
[2] Taeshi Koga, JFE Sekkei LTD, Tokyo, Japan, t-koga@jfe-sekkei.co.jp
[3] Yuto Kumon, Kagoshima University, Japan
[4] K. Otsuki, Kagoshima University, Japan
[5] K. Uchimura, Kagoshima University, Japan

them by haul trucks; and 7) CLT's slab–RGTSB composite beams.

In this paper, the connections for RGTSB members, experimental tests and numerical analyses on RGTSB column and beam under reversed cyclic load, are presented.

2 CONSTRUCTION AND CONNECTION

2.1 MAMNUFACTRUING PROCESS

Figure 2 shows manufacturing processes for RGTSB members. Deformed bars are casted into U-shaped grooves pre-cut in lamellas, which are arranged as outer lamellas in the member sections, and liquid epoxy resin adhesive is infilled into the grooves, pouring over the bars. The U-shape is formed in order to save the amount of the adhesive. The lamellas are formed by planer after the adhesive curing. The manufacturing process, after this, follows usual processes for Glulam timbers. The thickness of lamellas is formed to be 45mm; the width, to 210mm, corresponding to the maximum-size of lamellas in Japan. The maximum width of the beams is temporarily limited to 210mm in order to avoid secondary gluing. The bars are also limited to from D22 to D32; nominal diameter of D22 is 22mm; D32, 32mm.

2.2 CONSTRUCTION

Figure 3 illustrates an interior beams-column-foundation connection for two-way portal frames. The beams and the column are composed of RGTSB. The foundation is reinforced concrete (RC). The column section is configured a cross shape in order to resist to two-way forces in earthquakes and winds.
Figure 4 shows a framing elevation of prototype buildings. The column sections in building, are three types: +-shape, T-shape and L-shape as shown in Figure 5.

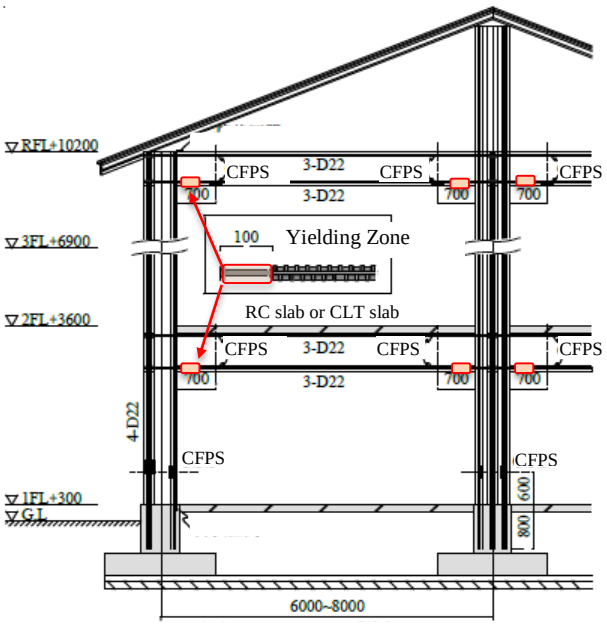

***Figure 4**: A framing elevation of prototype building; dimensions, arrangement of CFSP and Yielding zone*

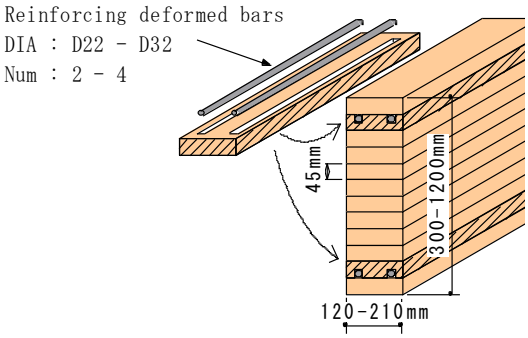

a) RGTSB making and dimensions

b) Inserted bars
Injecting adhesive

c) Bonding lamellas

***Figure 2:** Manufacturing process for reinforced timber using steel bars; RGTSB*

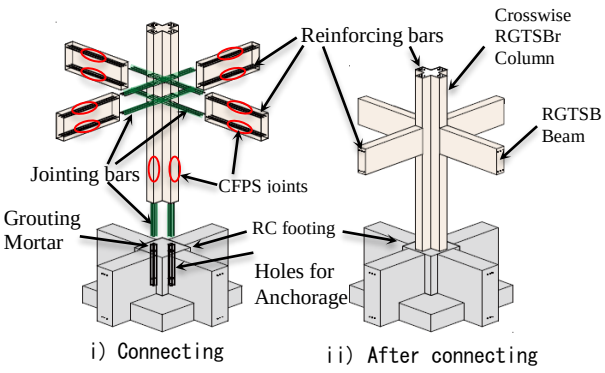

***Figure 3:** Beams-column-footings connections*

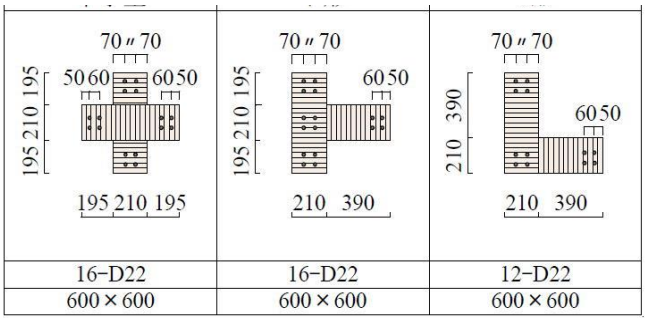

***Figure 5:** Cross-section types for column resisting tow ways 3-types: +-shape, T-shape and L-shape Dimensions: example, unite: mm*

The beams and columns are connected using glued-in deformed bars "*Jointing* bars" which are also jointed with the reinforcing deformed bars embedded in RGTSB beams, or columns connected to RC foundations, using carbon fibre plastic sleeves (CFPSs) and the same liquid epoxy resin adhesive as described in Sec.2.1. CFPSs are also embedded in RGTSB members at a certain distance from interfaces of the connections (Figure 4, 6).

2.3 CARBON FIBRE PLASTIC SLEEVS: CFPS

CFPS (Figure 6) and bars joint technique were developed by Shioya et al. [4], which can resist ultimate tensile strengths of deformed bars, without fracture of CFPS and bar pulling-out from CFPS.

Figure 7 schematizes CFPS configuration and section. CFPS is formed by rolling a carbon fibre sheet A1(four rolls) around a PVC pipe rolled a polypropylene(P.P.) tape spirally, arranging the longitudinal axis of the carbon fibres parallel to that of the pipe, and a carbon fibre sheet A2(four rolls) perpendicular to. The specific epoxy resin adhesive is applied to the sheets just before the rolling. The adhesive curing forms CFPS. After two deformed bars are respectively inserted into a CFPS as shown in Figure 6b, both the two bars are connected by injecting the liquid adhesive in sec. 2.1 , into a hole at the center of the sleeve and curing the adhesive.

Figure 8 shows stress-strain curves measured at tensile loading experiments on the connection of deformed bars (D22) using CFPS and the adhesive. The experimental parameter was development lengths of deformed bars in CFPS, which were 3d, 4d, 5d and 8d; d is nominal diameter of the bars, d=22mm. A stress-strain curve bold line of deformed bar D22 also shows in Figure 8 for comparing. Ultimate failures in specimens 3d, 4d, 5d, were pulling-out of deformed bars from CFPSs, however another bar in specimen 8d was fractured outside CFPS without the bars pulling-out. The tensile strength of the connection in 8d specimen would be found to be higher than the deformed bars. The elongation measure lengths were 320mm at the 3-5d, the D22 bar, and 440 mm at the 8d.

2.4 CFPS EMBEDMENT IN LAMELLAS

Figure 9 shows embedment for CFPSs in lamellas. The *reinforcing* deformed bars, which are inserted to the center of length in CFPS, are embedded together in lamellas. They are bonded to the lamellas by pouring the liquid epoxy resin adhesive over them. At the pouring, the liquid adhesive flows inside the clearance between the inner hole of CFPS and the inserted bar; both the *reinforcing* bar and CFPS are connected, after curing the adhesive.

On the other hand, at the other half of CFPS, no clearance between CFPS and PVC pipe, rolled the blue P.P. tape, is set, to prevent the adhesive from flowing inside. After the curing, the PVC pipe and the tape are pulled out; the end of lamella has holes in which jointing bars can be inserted and arrive at the end of the *reinforcing* bars in lamellas i.e. the center of CFPS.

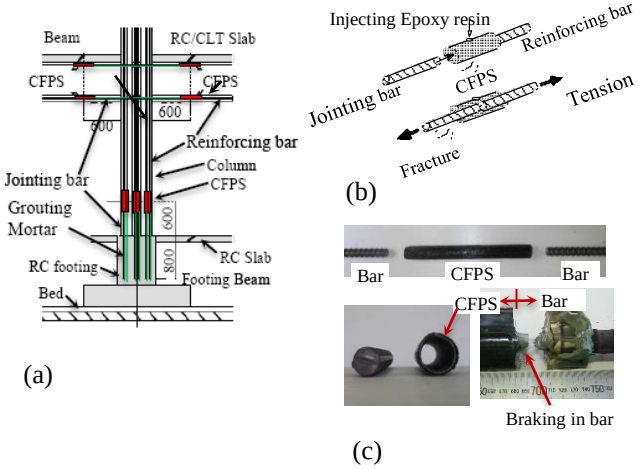

***Figure 6**: Schematizing CFPS positions and CFPS joint; (a)Arrangement of bars and CFPSs;(b) Joint of steel bars ;(c) CFPS and after tensile fracture*

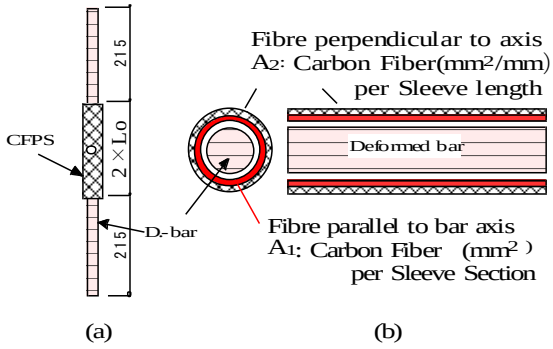

***Figure 7:** Schema for CFPS configuration and section:*

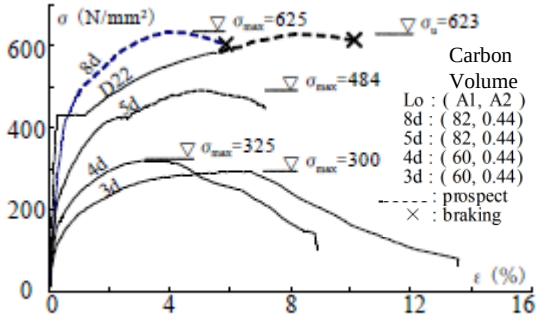

***Figure 8:** Stress-strain curves measured at tensile experiments on the connection of deformed bars (D22) using CFPS and epoxy resin adhesive.*

***Figure 9:** Embedding CFPS (black) in lamellas ;Bars (D22); PVC pipes rolled P.P.-tape (bleu)*

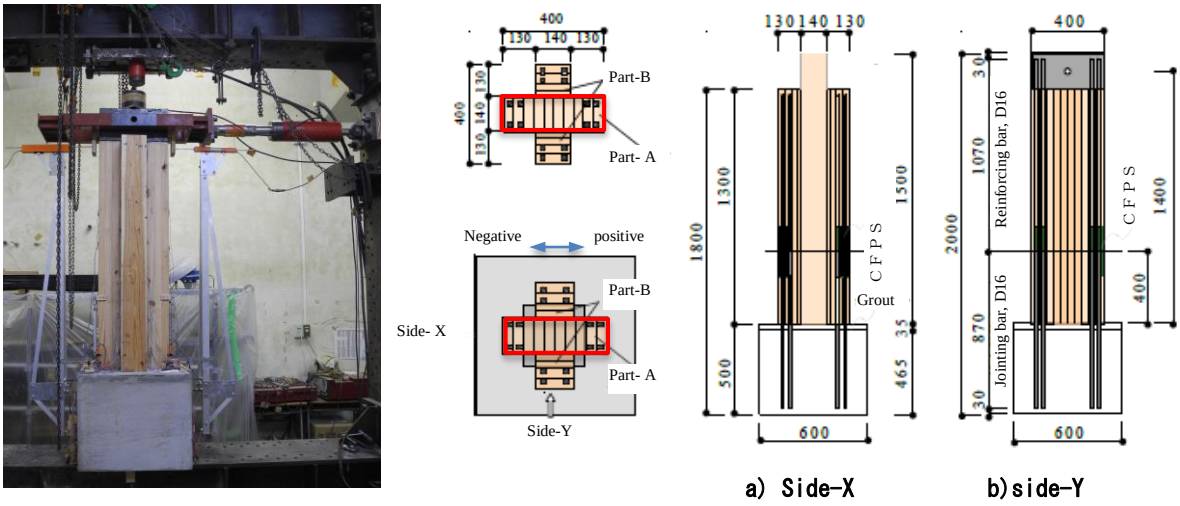

Figure 10: *Configuration of the column specimen*

3 EXPERIMENTAL TESTING OF COLUMN

3.1 SPECIMEN

A 2:3-scaled reinforced column tested. The configuration of specimen is showed in Figure 10. The specimen was modelled for a foundation and a column on the ground floor of building. The column section was a + shape; the ratio of reinforcement (8-D16) to the area (140mm x 400mm) of part A (see Figure 10) in the section was 2.8%. The length of CFPS at joint between the reinforcing bar and the jointing bar was 272 mm (i.e. 2x8.5x16mm) and the rolling of carbon sheets was performed according to the specification in Sec. 2.3. Figure 11a shows constitution of the column section. Part Bs were adhered to part A. The Glulam timbers of part A and B were laminated according to E65-F225 in Japanese Agriculture Standard. Table 1 shows mechanical properties of D16 and concrete in the specimen.

3.2 TEST SETUP AND LOADING

Figure 11b shows configuration of test setup for loading. Lateral force was cyclic reversed loadings with increasing the horizontal displacement of the top; vertical force at the top of the column was controlled to be constant 187kN. Figure 12 shows the displacement history at the top with the number of loading reverse cycles. The positive and negative peak displacements until the 18th cycle were controlled to be same magnitude, however, at the 19th cycle, quasi-static cyclic reverse loadings resembled free vibration to reveal re-centring ability of the column just after the bottom flexural yielded at earthquakes.
From the 35th cycle, again, lateral force was loaded with increasing the horizontal displacement of column.

3.3 RESULTS

3.3.1 FAILURES

Figure 13a shows lateral load-drift curves until 4% drift for the column; Figure 13b, the curves after the 4%. Figure 14 shows an envelopment curve of the lateral load-drift curves (bold curves). The failures were occurred in the following: 1) creaking sounds staring in timber, at So

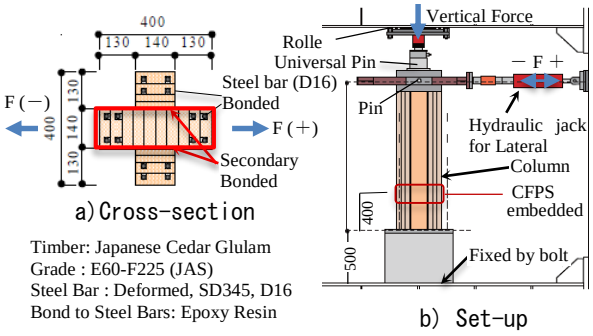

Figure 11: *Cross-section of Specimen and set-up*

Table 1: *Properties of deformed bars and concrete*

Material Property	(N/mm^2)
Deformed bar, D16	
Young's modulus	169000
Yielding stength	363
Tensile strength	605
Breaking strain	23%
Concrete, Fc42	
Specified desing compesive strength	42

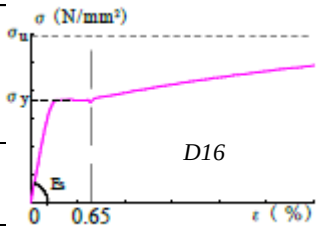

Tensile stress-strain curve

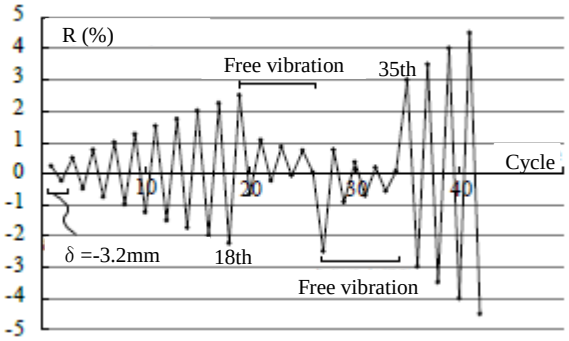

Figure 12: *Displacement history at top of column*

marked in Figure14; 2) tensile yielding of jointing bars between the column and RC foundation, at Y_1, Y_2; 3) small cracks on timber, at Cr_1, Cr_2, Cr_3 as shown in Figure

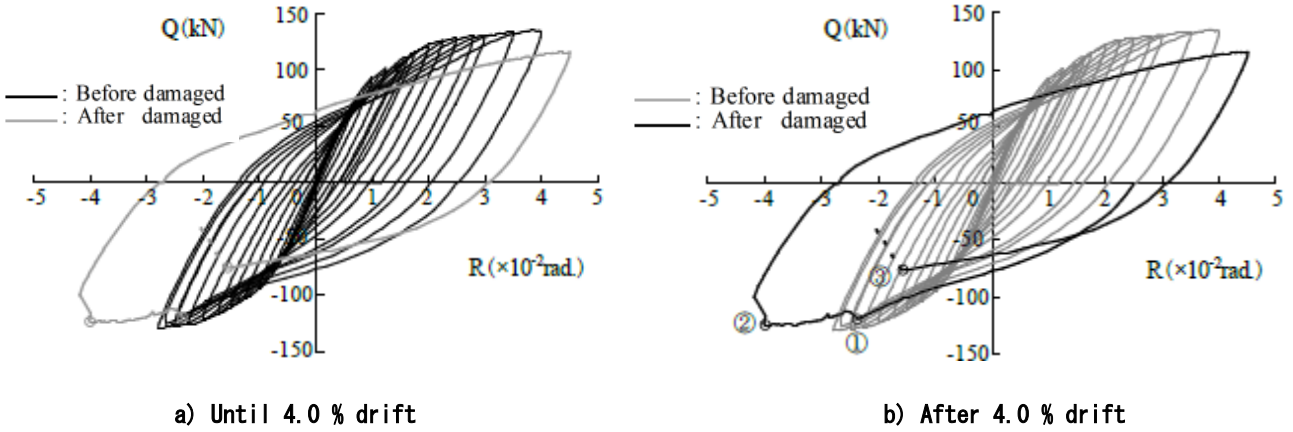

Figure 13: *Lateral load-drift curves*

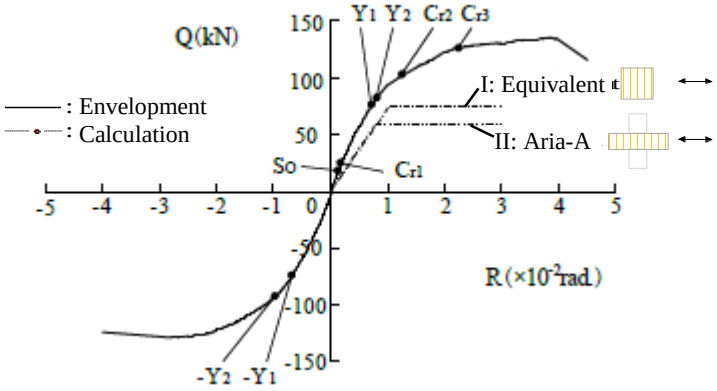

Figure 14: *Lateral load-drift envelopment curves*

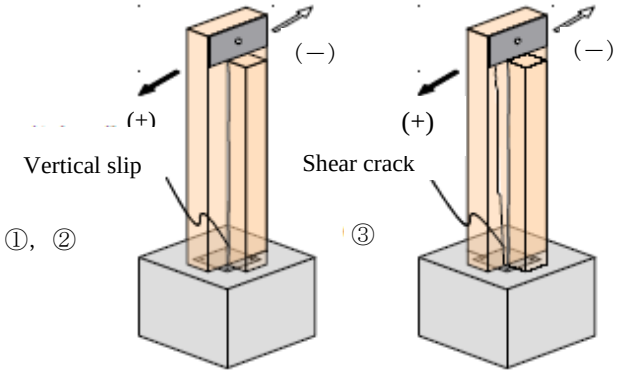

Figure 15: *Aspect of cracks at ultimate*

14; 4) shear failures with vertical cracks as shown in Figure 15. No damage necessary to repair in service of buildings occurred until the -2.4% drift. Also, no pulling-out of joint bars from the column and the foundation, except plastic elongation of the jointing bars, was observed: this suggests that CFPS joint performed such well as no-cut deformed bars.

The column yielded at its base by bending moment at 0.71% drift; shifted to secondary stiffness just after the yielding due to strain hardening of the jointing bars; exhibited strength near maximum load at 2.0 %; increased gradually to the maximum load until 4.0%. The hysteresis loops until 4% in Figure 13a, indicate spindle shapes with no pinching; performed abundant energy absorption as never observed in RC columns. In particular, the maximum load should be noted to be extremely higher than if the column had made using RC, because the jointing bars were near ultimate tensile strength at the maximum load.

Figure 16 shows an envelopment curve of relationship between slip displacements and the column-top displacements; the slips indicate some at the interface between the column base and RC foundation; the solid circles, ●, indicates the peaks of the cycle, the mean of the left-side hand and the right-side hand at the base of the column; blue line, 2%, the ratio of the slip to the displacement and red line, 4%; secondary abscissa, the drift in Figure 13. The slips were suppressed less than 2% of the column displacement until the 2% drift in positive loading and less than approximately 4% until the ±4% drift. These results support no pinching in the load-drift

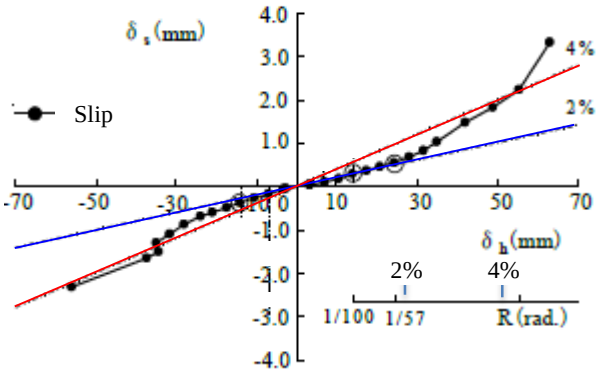

Figure 16: *Envelopment curve of relationship between slip displacement δ s and column-top displacement δ h*

curves in Figure 13a. We guess that the reinforcing bars in the part B (see Figure 10), performed, very well, as shear key.

3.3.2 RE-CENTRING AT LARGE DISPLACEMENTS

In vibration control structure building, secondary stiffness of the structure just after yielding of hysteresis damping device, reduces residual displacements of the building after earthquake i.e. performs re-centring ability. We, during loading in test, noted the secondary stiffness occurring on envelopment curve in Figure 14, due to strain hardening after yielding of jointing bars at the column base. We tested the secondary-stiffness effect to

minimize the residual displacements in the column, at the 19th cycle, in addition.

The final residual displacements of buildings after earthquake are reported to be less than them on assumption of free vibration after the maximum response, through dynamic numerical analyses on steel-structure building [5]. This suggests the residual drifts gained, by quasi-static cyclic reverse loading as free vibration, are safe in terms of minimizing residual displacement in buildings after earthquakes.

Figure 17 shows hysteresis loops in maximum drift=±2.5% cycles, measured by the quasi-static cyclic reverse loadings as free vibration; circles indicate final residual drifts; vertical broken line, allowable drift, 1/400, authors proposed to be visually negligible. The final residual drifts approached the allowable drift; this result demonstrates that column, using the connection proposed in Sec. 2.3, would have good re-centring ability by itself, under experience less than 2.5% drift.

4 EXPERIMENTAL TESTING OF BEAMS

4.1 DESIGN CONCEPT

The RGTSB column specimen in Sec. 3.1, connected to reinforced concrete foundation, performed well with extremely high stiffness, strength, energy dissipation, re-centering at drift 2%, never obtained in reinforced concrete columns. This suggests that RGTSB system would suppress responses of buildings in earthquake: damages, declines and failures of building, and therefore also minimize cost of the repairs. Moreover the high stiffness and strength would be sufficiently to wind loads in building-frame design. We have been developing a design methodology for 3-story buildings using RGTSB system, considering the requirements of fireproof building in Japan.

In RGTSB system, columns and beams consist of RGTSB members, using CFPS joint in beam-column connections and column-foundation connections in Chap. 2. Figure 18 shows frame hinges designed at big earthquake. Jointing bars in the column-foundation connections can obtain sufficient development lengths into the foundations. On the other side, at the columns, the jointing bars are connected to reinforcing bars embedded in the columns using CFPS. Therefore, the jointing bars can perform stiffness and ultimate strength in deformed bars: flexural hinge at bottom of the columns would perform high strength and energy dissipation.

On the other hand, column-beams connection requires capping maximum bending moment at the column-beam interfaces, for avoiding development failures of the joining bars and shear failures in column-beam joint panels.

4.2 CAPPING BENDING MOMENT AT HINGS

Stiffened adhesive around jointing bars would be thought to restrain deformations in the bars after yielding; the restrain limits zones at which the plastic strain occurs in the bars; therefore, the strain hardening would occur at comparative slight drift; the secondary stiffness on load-displacement curves, was thought to occur at the

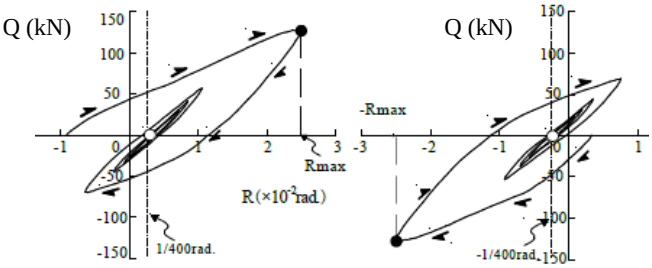

Figure 17: *Hysteresis loops at 2.5%, by quasi-static cyclic reverse loadings similar to free vibration*

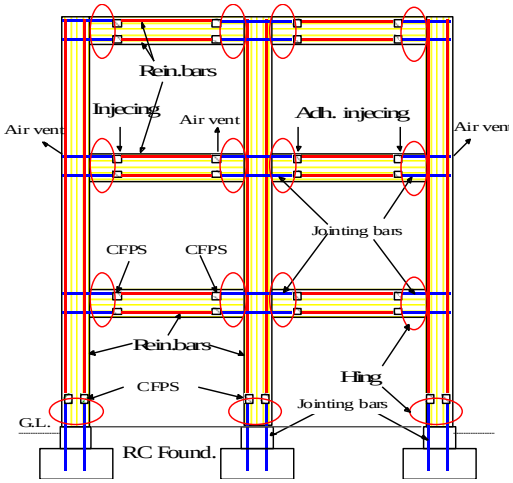

Figure 18: *Frame hinges designed at big earthquake*

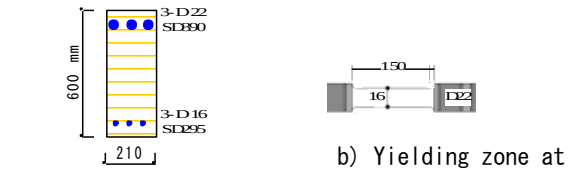

Figure 19: *Capping concepts for maximum bending moment at beam ends*

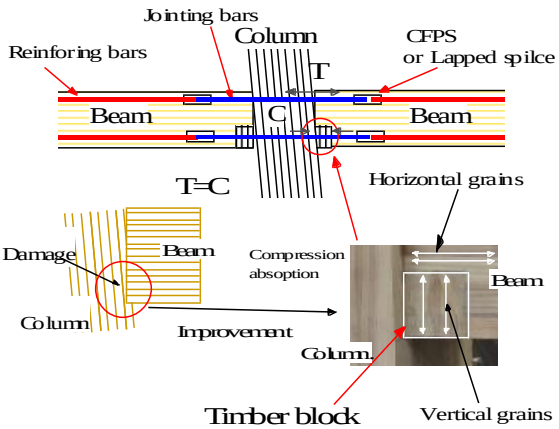

Figure 20: *Timber block for compression-deformation absorption at beam-end bottom*

approximate 0.7% drift described Sec. 3.3.1, just after flexural yielding at the beam ends, and the jointing bars would develop ultimate strength of themselves at drift 2.0%. Then, at the column-beam connection, bar-development failures and panel-shear failures would

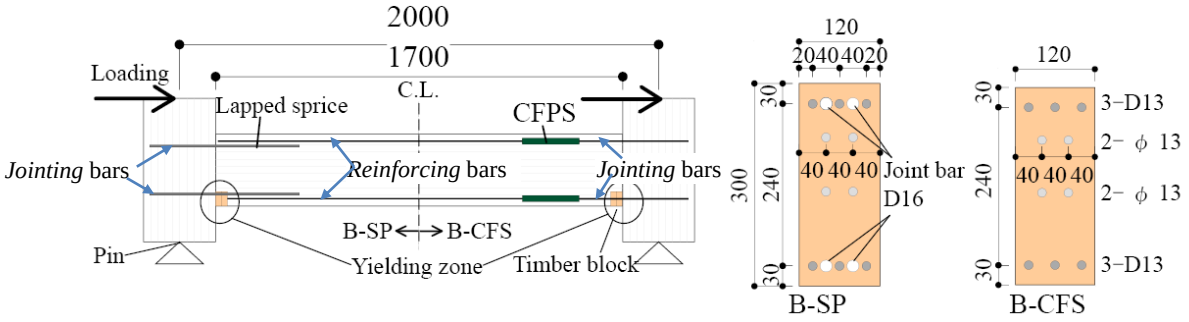

Figure 21: *Configuration and beam end sections*

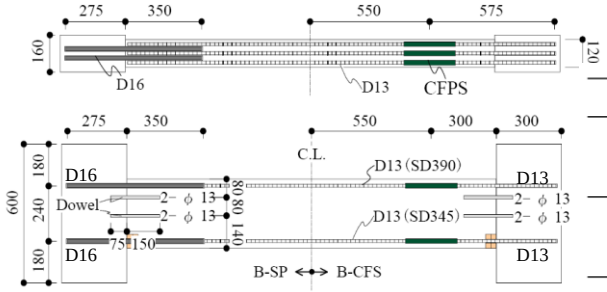

Table 1: *Properties of deformed bars*

		a mm²	Es ×10⁵	σ_y N/mm²	ε_h %	σ_u N/mm²	ε_m %
D13	yielding zone	62.2	1.93	410	1.27	637	–
	SD345	126.7	1.87	378	1.20	564	–
	SD390	126.7	1.75	426	0.84	667	–
D16	yielding zone	95.0	1.89	389	0.68	651	–
	SD345	198.6	1.70	372	1.04	599	–
	SD390	198.6	1.82	413	0.85	645	–

※ : yielding zone is actual cross-section area, the others are nominal cross-section area.

a : cross-section area (※)
σ_y : yield strength
σ_u : tensile strength
Es : young's modulus
ε_h : modulus of strain hardening
ε_m : strain at tensile strength

Figure 22: *Specimen dimensions, dowel round steel bars*

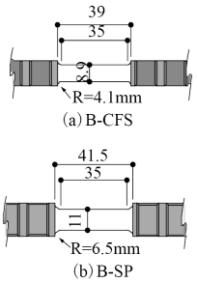

Figure 23: *Dimensions of yielding zone at bottom bars*

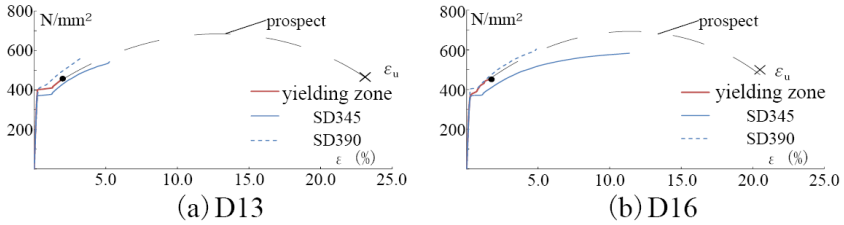

Figure 24: *Tensile stress-train curves at yielding zone*

occur easily because resultant force of top or bottom jointing bars increase.

Capping maximum of the resultant force is required in order to prevent the failures.

Turning down jointing bars, at beam-column connection using glued-in rod, has been already developed in Japan [6], and also developed as energy dissipation device in Post-Tensioned Timber Frames [7]. These concepts applied at both upper and bottom at beam ends.

We expected that decreasing the amount of bottom jointing bars than the top jointing bars would be efficient to cap the resultant forces, because the resultant force of the bottom bars is equal to that of the top bars; this concept would bring three merits; to prevent flexural stiffness at beam ends from decreasing due to turning down upper jointing bars; to cut costs of turning down upper jointing bars; moreover, to prevent beam deflection in service from increasing after degrading flexural stiffness of the beam ends due to top jointing bars yielding in earthquake. Herein, we applied turning down at a zone on only bottom jointing bars, yielding zones, instead of decreasing the amount of bottom jointing bars.

Longitudinal deformation of the bottom jointing bar would be thought to be larger, in case of letting not to yield the top jointing bars. This situation makes the bottom edge at beam ends thrust the connected timber column perpendicularly to the grain and damage to the column.

In order to prevent the damages, we bonded glulam timber blocks to pre-cut bottom edge zones at the beam ends, with setting the block grain parallel to the column axis, using epoxy resin adhesives; designed the timber blocks to absorb compressive deformation at the edge.

4.3 SPECIMENS

Two RGTSB-beam specimens scaled down at 1:2, B-SP, B-CFS, tested. Figure 21 schematizes configuration of the specimen, arrangement of reinforcing bars and jointing bars, loadings and supporting. The specimens were RGTSB beam- glulam-timber columns assemblies. Figure 22 shows specimen dimensions, dowel round steel bars at the column-beam interface, and positions of CFPS. Three D13 deformed bars were embedded at both upper and bottom in the beams, D13; nominal diameter, 13mm. The upper bars were SD390 in grade; the bottom bars were SD345.

The column-beam connections were applied using the jointing bars and epoxy resin adhesive described in Sec. 2.3. The column-beam interfaces, sealed around from the outside, were infilled with the adhesive, when injecting the adhesive into the jointing bars in specimens.

In B-SP specimen, *jointing* bars(2-D16) and *reinforcing* bars(3-D13) in the beam were connected using lapped

splice transferring force at wood between the jointing bars and the reinforcing bars bonded in beam; in B-CFS specimen, jointing bars(3-D13) and reinforcing bars(3-D13) were connected using CFPS joint in Sec. 2.3.

Side faces of the columns, front and back in Figure 31, were strengthened, by bonded steel plates with epoxy resin adhesive, because cracks was observed to indicate shear failure in column, during loading in B-SP in Figure 34a. B-CFS was also strengthened before loading; therefore no crack on the columns was observed. Two round steel bars, as dowel shear keys, were inserted at each column-beam interface, into holes at columns and beam, and the liquid epoxy resin adhesive(in Sec.2.3) was injected into the holes inserted the dowels, at the same time injecting the adhesive to the jointing bars.

The column-side parts of the dowels were coated with water paint for preventing the dowel in tensile.

The Glulam timbers were laminated according to E65-F225. Table 1 shows mechanical properties of deformed bars. Figure 23 shows dimensions of turned down zone, yielding zone, on jointing bars, designed to fracture the zone without yielding except yielding zone, based on preliminary test.

Figure 24 shows tensile stress-train curves measured at yielding zone and deformed bar by test piece, respectively.

Figure 25 shows detail and dimensions of the timber block at the bottom edge of beam ends. The blocks were bonded to tow interfaces on beam, with an epoxy resin adhesive. Figure 27 shows compressive stress-strain curves measured in compressing test for block specimens. Figure 26 schematizes configuration and loading to the block specimens.

4.4 TEST SETUP AND LOADING

Figure 28 shows configuration of test setup for loading. Vertical forces were cyclic reversed loadings with increasing vertical displacement in between the left-hand side column and the right-hand, adjusting the rotation angles of both columns to be equal, by vertical tow actuators. Figure 29 shows displacement history with the numbers of loading cycle.

The positive peaks and negative of the displacements were set to be same. From the 5 cycle, quasi-static cyclic reverse loadings (QCRLs) similar to free vibration, were conducted to reveal re-centering ability in the beams due to residual vibrations just after maximum response at big earthquake.

At the 11th cycle, the peak was maintained to 1.0% drift, taking account for aftershocks following main earthquake; QCRLs were, again, conducted with increasing the peak to the final.

4.5 RSULTS

4.5.1 SHEAR FORCE-DRIFT CURVES AND FAILURES

Figure 32 shows vertical shear force-drift curves until first 2.0% drift in beam; Figure 33, from the 2nd 1.0% drift, for the aftershock, to the final. The shear force is the sum of those of the two actuator; the drift is vertical displacement over beam clear span. Figure 34 shows aspect of failures at the final.

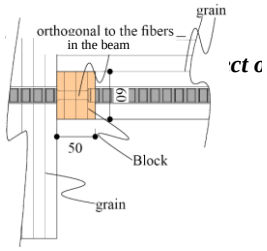

Figure 25: *Dimensions of timber block*

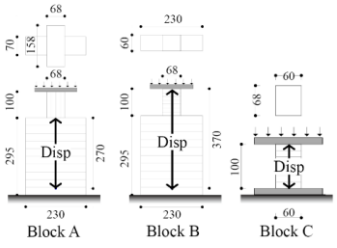

Figure 26: *Configuration of block specimens and loading*

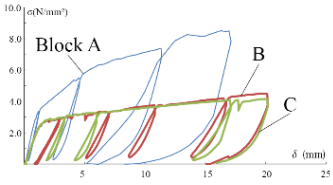

Figure 27: *compressive stress-strain curves of the block*

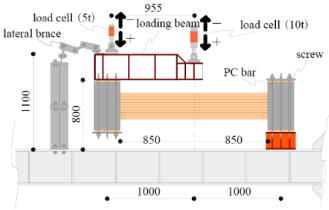

Figure 28: *Test setup for loading.*

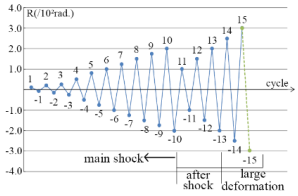

Figure29: *vertical displacement history*

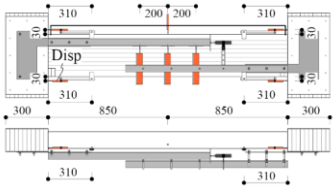

Figure 30: *Inductive Displacement Transducers arrangement*

Figure 31: *Configuration of setup and loading*

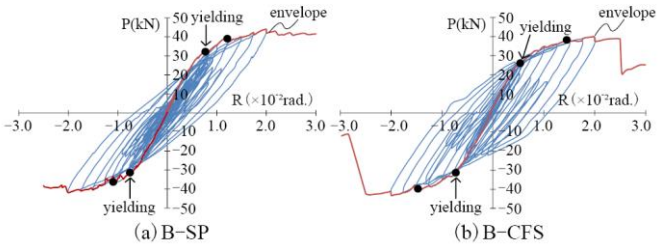

Figure 32: *vertical shear force-drift curves until the first 2.0%*

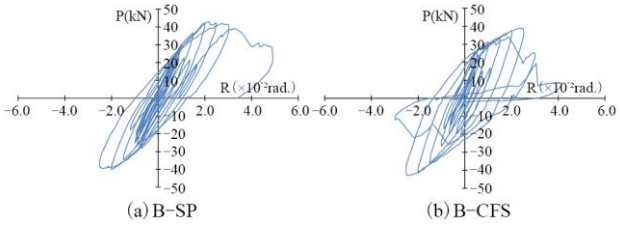

Figure 33: *vertical shear force-drift curves from the 2nd 1.0% to the lastl*

B-SP specimen: lapped splice joint

Tensile yielding or compressive yielding in the yielding zone on bottom jointing bars at both beam ends, simultaneously occurred at 0.62% drift. From this drift, the stiffness on the envelopment curve (red line) shifted to the secondary stiffness; the third stiffness, at 1.27%; the third was remained to 2.0%. Tensile yielding in upper jointing bars at beam ends caused shifting to the third. Envelopment curve for the aftershock loading (see Figure 33a) also indicated the secondary stiffness from 1.0% to 2.0%. Vertical shear cracks were observed in the left-side hand column (Figure 34a), at +2.06% in the +14th cycle; the strength remained until 3.1%, however, development failure occurred at woods around the upper jointing bars in the column sides; the later loading degraded the beam. No fracture at the yielding zones occurred.

B-CFS specimen: CFPS joint

Tensile yielding or compressive yielding in the yielding zones on bottom jointing bars, also simultaneously occurred at 0.53% drift. From this drift, the stiffness on envelopment curve shifted to the secondary stiffness; the third, at 1.50%; the third was also remained to 2.0%. Upper jointing bars did not yield until the last. Envelopment curve for the aftershock loading (Figure 33b) also indicated the secondary from 1.0% to 2.0%. Strength at the 2.0% remained until 2.5%, however, yielding zone on bottom jointing bars was fractured in tensile at 1.9% in the +15 cycle, peak 3.0%; bottom timber part was separated from beam, at -0.7% in the -15 cycle, peak -3.0%, as shown in Figure 34b.

4.5.2 DAMAGES IN TIMBER BLOCKS

Figure 35 shows aspects of a timber block at beam end under compression or tensile in B-SP. Noticeable damages were not observed at the blocks under compression, however, vertical crack parallel to grains in the block occurred under tensile. Figure 36 shows relationship between beam shear force and horizontal deformation in the block, at the block mid-height. Negative deformations under compression were not increased such as those of block B, C in Figure 27. This suggests that beam timber parts on the blocks thrust to column at the column-beam interfaces. Improvement on the block dimensions would be necessary, corresponding to target drifts in design.

4.5.3 Re-centering

Figure 37 shows hysteresis loops in the 10th positive cycle, maximum drift=+2.0%, measured in the quasi-static cyclic reverse loadings as free vibration; circles indicate the final residual drift, Re; solid circle, the first residual drift, R1 at the first time when the force is zero just after the peak in cycles. Re of B-SP was more conservative than that of B-CFS and near the allowable drift (1/400rad. in sec.3.3.2), however B-CFS exceeded the value. This cause is thought to have been buckled at the yielding zone in bottom bar. This phenomenon needs more consideration.

Figure 38 shows the residual drift (Re, R1)–peak drift relationship at the cycle as free vibration: solid lines

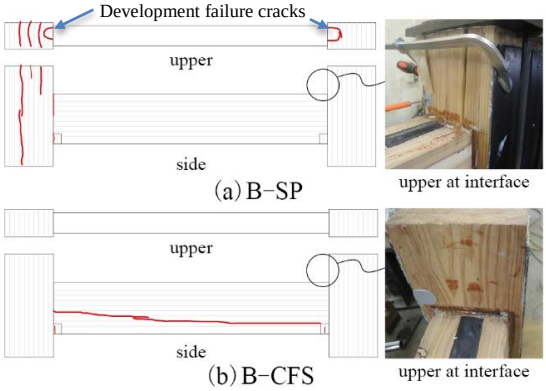

Figure 34: *Aspect of failures at the final*

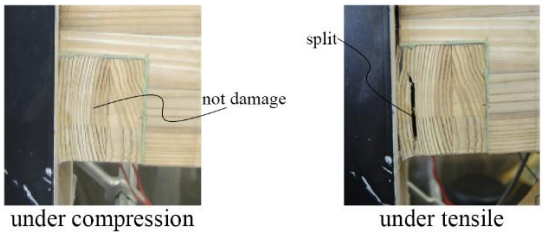

Figure 35: *Aspects of failures at the beam-end in B-SP*

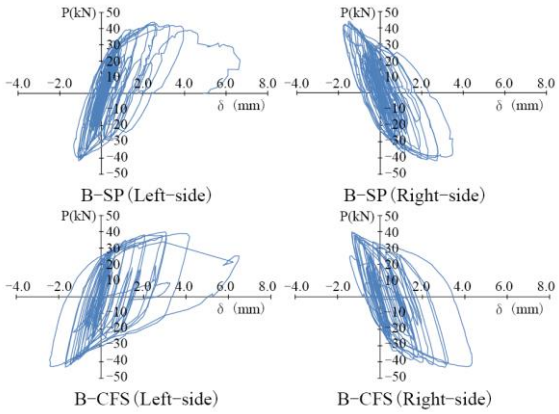

Figure 36: *Relationship between beam shear force and horizontal deformation at the timber block*

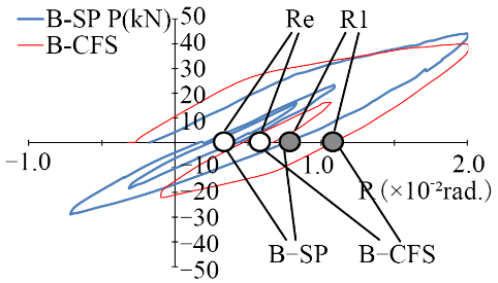

Figure 37: *Hysteresis loops at positive 2.0 %, by quasi-static cyclic reverse loadings similar to free vibration*

indicate Re; dotted line, R1. B-SP suppressed more efficient residual drift than B-CFS.

5 Numerical analysis

Hysteresis loops until peak load were obtained using an application software for reinforced concrete model, member and structure SNAP. Hinge lengths at the column bottom and the beam ends in specimens were

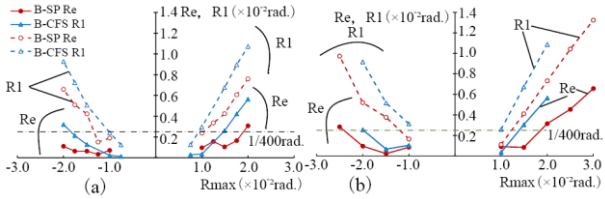

Figure 38: *Residual drift – peak drift in cycles: (a) until the first 2.0%; (b) from the 2nd 1.0% to the last*

assumed to be equal to the depth in them, respectively: 400mm in column; 300mm in beams. Bending moment and curvature in the hinge were assumed to be constant and elastic-plastic, such as stress-strain curves in Figure 39.

Figure 40 shows comparison between analysis and experiment on Hysteresis loops (shear force-drift) in the column specimen in sec.3.1 [8]; Figure 41 shows comparison between analysis and experiment on Hysteresis loops (shear force-drift) in Beam B-CFS. Analysis method for reinforced concrete members and structure is referred to sufficiently effective in RGTSB.

6 CONCLUSIONS

One reinforcement technique RGTSB for the low-grade Japanese cedar's glulam timbers and the building construction using it was presented. The column and the beam composed of RGTSB performed higher stiffness, strength, ductility, dissipation than RC members. The numerical analysis using an application software for RC structure, predicted the load-drift loops of until failure of the experimental test.

REFERENCES

[1] M. Kaestner, W. Haedicke, M. Jahreis,K. Rautenstrauch: High-tec timber beam–a high performance properties. In: Proceedings of the World Conference on Timber Engineering WCTE 2014, Quebec City,Canada, 2014.

[2] S. Goto, M. Tokuda, T. Uchizako: Creep of hybrid composite timber beam, The 47th Annual Meeting of the JWRS, No.4915:196, 1997 (in Japanese).

[3] N. Yamad, S. Shioya: An Reinforced Timber Assemblies by Reinforcing Steel Bar, AIJ Kyushu Chapter Architectural Research Meeting, No.49:613-616, March 2010 (in Japanese).

[4] T. Koga, S. Shioya, et al.: Timber Frame Structure Reinforced by Reinforcing Steel Bar. Part2, AIJ Kyushu Chapter Architectural Research Meeting, No.51, 590-563, March 2012 (in Japanese).

[5] T.Kidowaki, K. Inoue: Residual deformation of one-freedom-bilineal-system under strong earthquake, Summary of technical papers of annual meeting, p.p.935-936, Sept. 1999 (in Japanese).

[6] H. Ito, M. Shiozaki. H.Takahashi., Y. Ohashi: Development of glues-in rod joint having ductile region, Summary of technical papers of annual meeting, p.p.545-9546,Sept 2012(in Japanese).

[7] T. Armstrong, T. Smith, et al.: Seismic detailing of post-tensioned timber frames, In: Proceedings of the World Conference on Timber Engineering WCTE 2014, Quebec City,Canada, 2014.

[8] R. Kawabe, Y. Kumo, S. Shioya, et al.: Prediction for Horizontal Load-Displacement Relationship of Column and Hysteretic loop, AIJ Kyushu Meeting, No.54, 745-748, March 2015 (in Japanese).

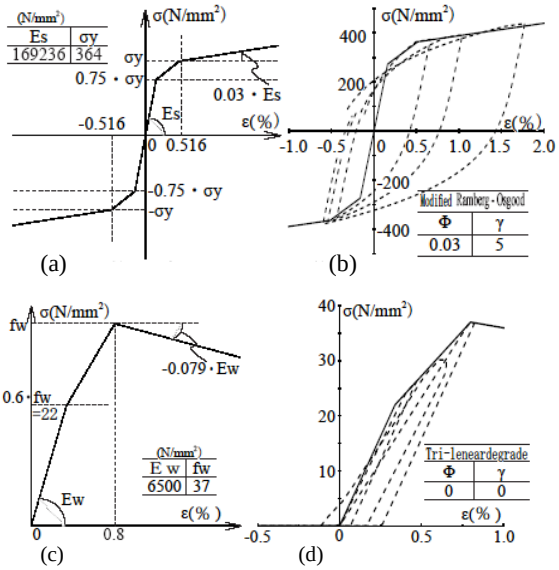

Figure 39: *Assumed stress-strain curves :(a)steel envelopment;(b) steel reversed lading;(c) timber envelopment in compression; (d) timber reversed lading cycles*

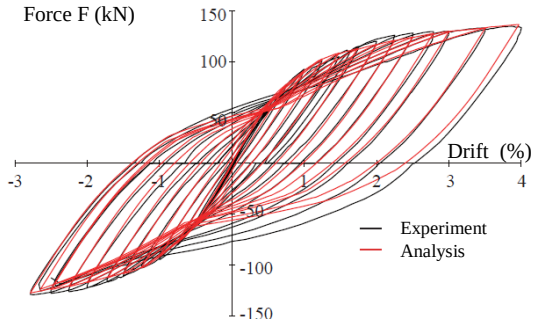

Figure 40: *Comparison between analysis and experiment on Hysteresis loops in the column specimen in Sec. 3.1*

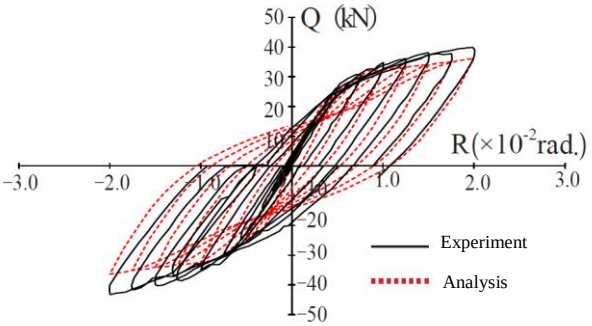

Figure 41: *Comparison between analysis and experiment on Hysteresis loops in Beam B-CFS in Sec. 4.3*